Electronic Supplementary Material (ESI) for Journal of Materials Chemistry B.

Shape memory polyurethane potentially used for vascular stents with water-induced stiffening and improved hemocompatibility

Ruibo Yang,[a] Wenkai Liu, [a] Ao Wang, [a] Xiaobo Deng, [a] Yuan Feng, [a] Qiao Zhang,[*b] Zhen Li, [* a] Feng Luo, [a] Jiehua Li, [a] and Hong Tan[*a]

[a] College of Polymer Science and Engineering, State Key Laboratory of Polymer Materials Engineering, Med-X Center for Materials, Sichuan University, Chengdu 610065, China.

[b] Department of Neurosurgery, West China Hospital, Sichuan University, Chengdu 610065, China.

Characterization methods

M1. DPD simulation method[1-5] The DPD simulations were performed by MS 7.0 in a cubic box with 3D periodic boundary conditions, containing 1.92×10^5 beads at $\rho = 3$ to avoid the finite size effect. Volume fractions of water beads (1%) were designed for TAPU1020. The r_c is 0.71 nm and the box size is 28.46 × 28.46 × 28.46 nm. The spring constant C = 4 and the thermal energy $k_BT = 1.0$, the friction coefficient γ and the noise amplitude σ were set as 4.5 and 3.0, respectively. The simulation duration was 1×10^5 and the time step was set as 0.05 τ . The equilibrium states were confirmed through monitoring the pressure, temperature, and morphologies. More detailed information is as follows.

Dissipative particle dynamics (DPD) simulation can be of great convenience to illustrate the mesostructure of the materials. Obtaining bead-bead repulsion parameter (α_{ij}) is one of the most important aspects of DPD. The α_{ij} could be calculated by

Flory-Huggins parameter(χ_{ij}) as

$$\alpha_{ij} = \alpha_{ii} + 3.27\chi_{ij} \quad (1)$$

α_{ii} is usually set as 25 in a density of 3 DPD units. The χ_{ij} can be obtained from

$$\chi_{ij} = (\delta_i - \delta_j)^2 \frac{V_m}{K_B T} \quad (2)$$

Where V_m is the average molar volume and the δ is Hildebrand solubility parameter, which corresponds to cohesive energy (E_{coh}) and cohesive energy density (CED) and can be calculated by

$$\delta = \sqrt{\frac{E_{coh}}{V}} = \sqrt{CED} \quad (3)$$

Using Materials Studio (MS) 7.0, successive all-atom molecular dynamics (AAMD) simulations were conducted in boxes containing 10 same beads constructed by the Amorphous Cell module. The AAMD was carried out in a 1 ps equilibration step followed by 100 ps NVT ensemble with COMPASS force field. δ and CED were derived from MD trajectories by CED calculation tool in the Forcite module package. Table S5 lists the solubility parameter of the beads. Table S6 lists the α_{ij} calculated by Eqs.**(1)-(3)**. Main chains beads A, B, A_2 and D along with side chains beads D, E and F and water beads W as well as coarse-grained models of TAPU1020 are shown in Fig. S17.

M2. MD simulation method[6] All models were constructed and the simulations were performed by Materials Studio software with a condensed-phase optimized molecular potentials for atomistic simulation studies (COMPASS) force field.[7] Three-dimensional periodic boundary conditions were applied to the amorphous cell, while in the 3D micro-crack model, the periodic boundary conditions were applied in XY direction, and the non-periodic fixed boundary conditions were applied in the Z direction. The Newton equation of motion was integrated by verlet algorithm[8] with the time step of 1 fs. The Andersen barostat[9] and the Nose thermostat[10] were

employed to control pressure and temperature, respectively. The electrostatic interactions were calculated by the Ewald summation method and the van der Waals interactions were calculated by Lennard-Jones function. The cutoff distance of nonbonded interactions composed of electrostatic and van der Waals components is 12.5 Å.

The amorphous model was subjected to 500 ps of the NVT ensemble and then 500 ps of NPT ensemble to obtain the final micro information. Fractional free volume (FFV) can characterize the packing ability of polymer chains and be calculated by $FFV = \frac{V - V_0}{V}$, where V is the total volume and V_0 is the occupy volume approximately equal to 1.3 times van der Waals volume. The radius of the Connolly probe used in calculating the atom volume field was set to 1.0 Å.[11]

Mean square displacement (MSD) analysis is a technique which determines the mode of displacement of particles followed over time. In particular, it can help to determine whether the particle is freely diffusing, transported, or bound.[12]

$$MSD = \left\langle \left| r_i(t) - r_i(0) \right|^2 \right\rangle \quad (4)$$

where $r_i(t)$ is the position vector of atom at time t, and $r_i(0)$ is the initial position vector, and the bracket expresses the ensemble average. The calculation of MSD is based on the average of the square of the distance difference between all atoms at Δt interval. The distance difference at Δt interval is obtained based on the atomic coordinate. That is, if there are N equivalent particles, the MSD can be averaged further:

$$MSD(\Delta t) = \sum_{i=1}^{N} MSD_i(\Delta t) \quad (5)$$

Therefore, the MSD for polymer chains is the mean value of the MSD of all atoms. Then the MSD for different systems can be compared even if they have different molecular weights (chain lengths or the number of atoms). In addition, MSD analysis can derive an estimate of the parameters of movement, such as the diffusion coefficient (D) for freely diffusing particles. The MSD as a function of the time

interval Δt typically increases quadratically at short time intervals (ballistic regime). If the particle is bound the MSD levels off to a constant. If the particle is diffusing, the MSD becomes linear in time; the slope defines the D, according to the Einstein equation.[13]

$$D = \frac{1}{6}\lim_{\Delta t \to \infty} \frac{d_{MSD}}{d_{\Delta t}} \qquad (6)$$

MSDs of main chains and side chains as a time function are presented in Fig. S11.

M3. Platelet adhesion and activation. Fresh human blood was centrifuged at 1000r/min for 15 min to obtain platelet-rich plasma (PRP). All the samples were immersed in PBS (pH = 7.4) for 12 h and then placed in a 96-well plate. 200 μL PRP was added to each sample and incubated for 2 h at 37 °C. The quantity and morphology of platelets adhered on PUs was observed by SEM. Briefly, the adherent platelets were immobilized with 2.5% (v/v) glutaraldehyde in PBS solution for 1 h, dehydrated with gradient ethanol, and subjected to critical point drying for SEM assay.

M4. In vitro coagulation time tests. Fresh human blood was centrifuged at 2500r/min for 15 min to obtain platelet-poor plasma (PPP). All the samples were immersed in PBS (pH = 7.4) before incubating with PPP. The effects on coagulation in the presence of PUs were studied after mixing anticoagulated blood plasma with the sample in the cuvette strips at 37 °C for 30 min before adding the coagulation reagents. PPP was acted as the control. All the assays were performed and measured using an automated coagulation analyzer (CA-530, Sysmex, Japan). All the coagulation tests were performed in triplicate.

M5. Histocompatibility assessment. PUs were cut into circular shape and subcutaneously implanted into Sprague Dawley (SD) rats. The rats were euthanized at 7d and 14d after surgery and the materials and adjacent tissues were collected. H&E

staining was used to access the tissue response. All care and handling of animals were performed with the approval from the Ethics Committee of West China Hospital, Sichuan University and in accordance with the Principles of Laboratory Animal Care of the National Institute of Health, China. (Approval Number 20211702).

M6. Staining and the simulation of the process of soft-to-stiff transition combined with shape recovery in vivo. The square ring was formed by adding thymol blue with a mass fraction of 0.1% in the DMF solution of TAPU1020 and forming into a film, cutting it into a 1.5 * 9 cm rectangular strip, folding it into a square ring, and bonding the interface with glue. The square ring was put in a 23 °C thermostat for 24 hours, and then a weight of 8.5g was placed on the square ring at room temperature. Next, the square ring was put in an 80 °C oven, folded into half to obtain a temporary shape, and fixed at 0 °C for 10 minutes. Then, the square ring was immersed in 37 °C warm water to restore its permanent shape after the temperature was recovered. After the shape of the square ring was basically unchanged, the square ring was taken out and refolded to its original shape quickly. The same weight was placed on the square ring and the degree of compression of the square ring was record. R_r of TAPU1020 in 23 °C water is 68.2 ± 2.4 %, while it is 66.8 ± 3.2 % after dyeing with thymol blue. The effect of the trace addition of thymol blue on the shape memory performance can be ignored.

Supporting Figures and Tables

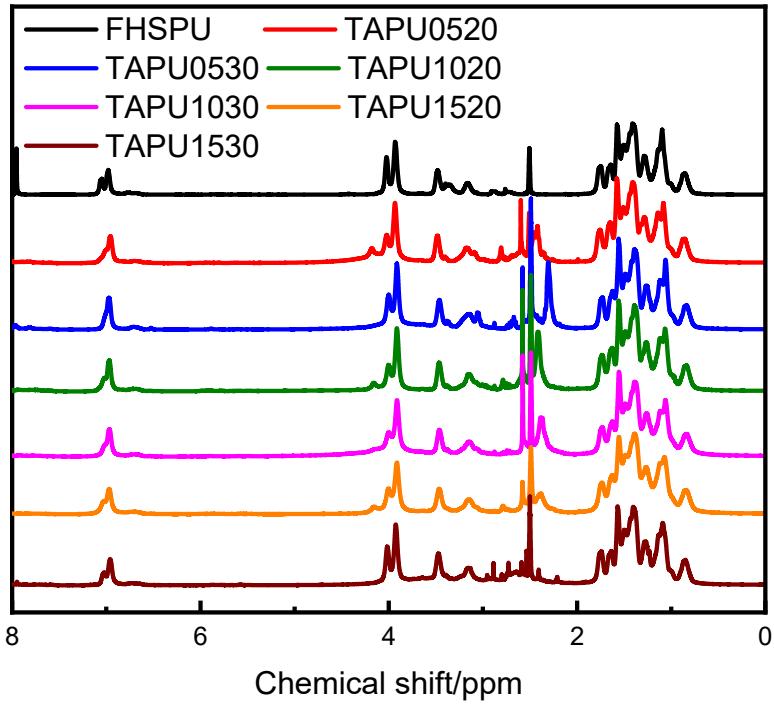

Fig.S1 ^{1}H-NMR spectra of TAPUs and FHSPU.

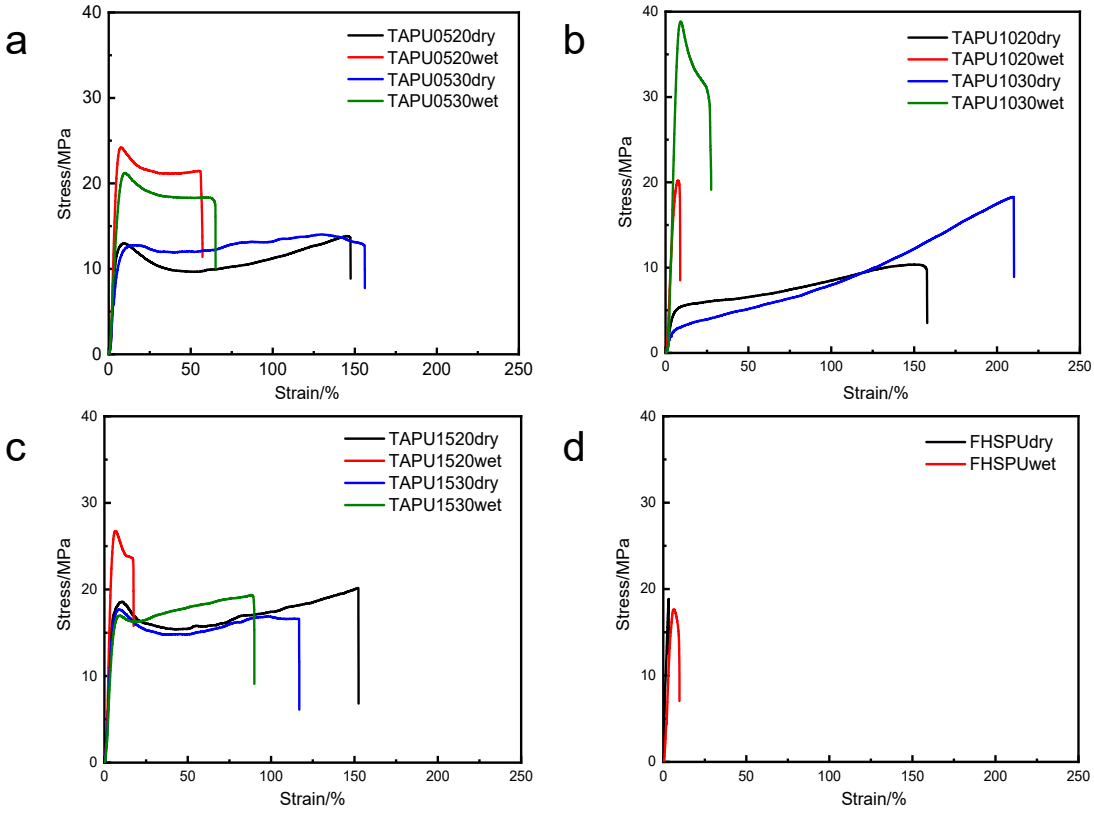

Fig. S2 Stress-strain curves for FHSPU and TAPUs for dry and hydrated samples at room temperature (23 °C).

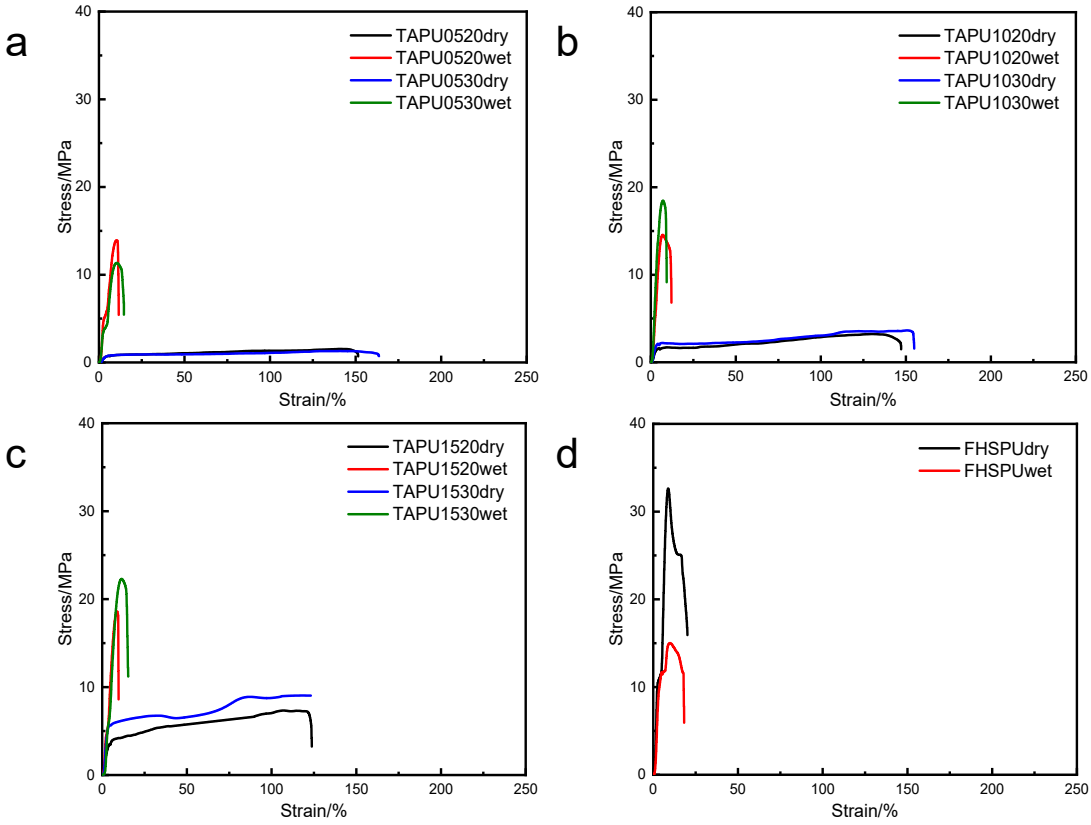

Fig. S3 Stress-strain curves for FHSPU and TAPUs for dry and hydrated samples at physiological temperature (37 °C).

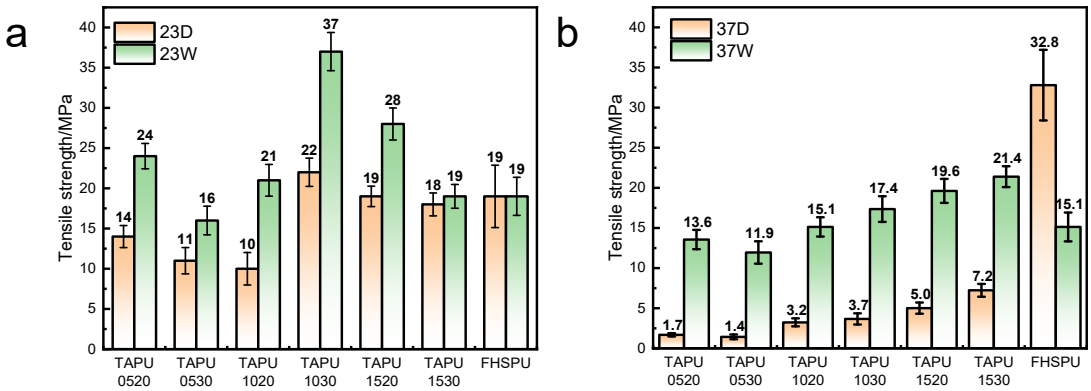

Fig. S4 (a) Tensile strength of FHSPU and TAPUs before and after absorbing water for 1d at 23 °C. (b) Tensile strength of FHSPU and TAPUs before absorbing water and after absorbing water for 1d at 37 °C.

Table S1 Shape fixation ratio (R_f) and Shape recovery ratio (R_r) of TAPUs.

Sample	R_f	R_r			
		23D	23W	37D	37W
TAPU0520	100±0.0	8.3±3.7	45.3±2.1	29.7±5.2	75.3±3.0
TAPU0530	100±0.0	7.6±3.4	52.8±2.7	32.6±4.5	74.5±3.4
TAPU1020	100±0.0	13.2±3.7	68.2±2.4	34.7±4.3	89.6±4.2
TAPU1030	100±0.0	14.9±3.8	73.8±3.3	39.0±5.6	95.9±3.3
TAPU1520	100±0.0	22.6±4.7	79.0±3.6	42.1±5.5	100±0.0
TAPU1530	100±0.0	25.8±4.2	84.3±3.3	46.3±4.2	100±0.0

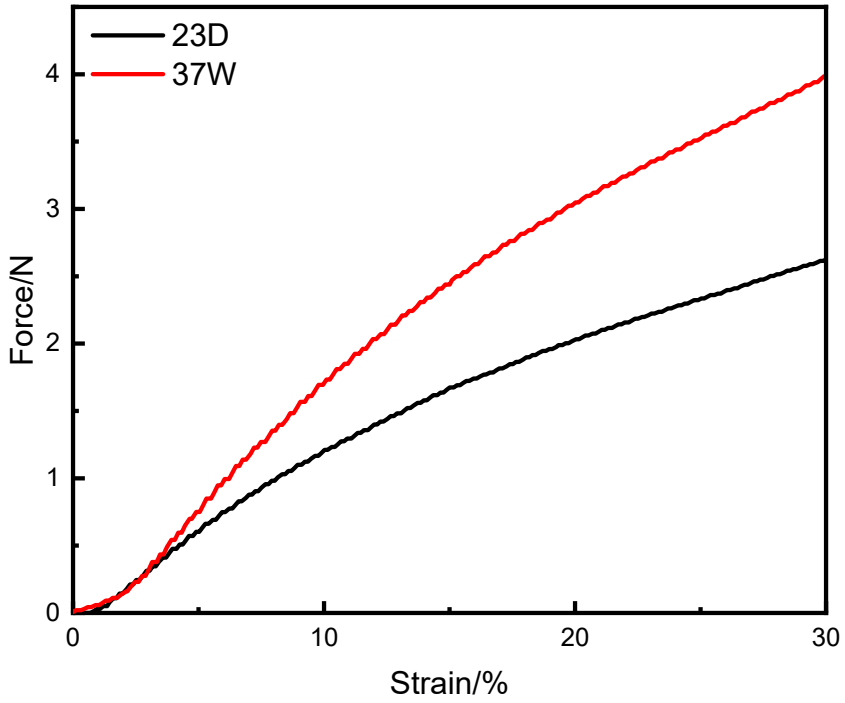

Fig. S5 Compression resistance of the stent made of TAPU1020.

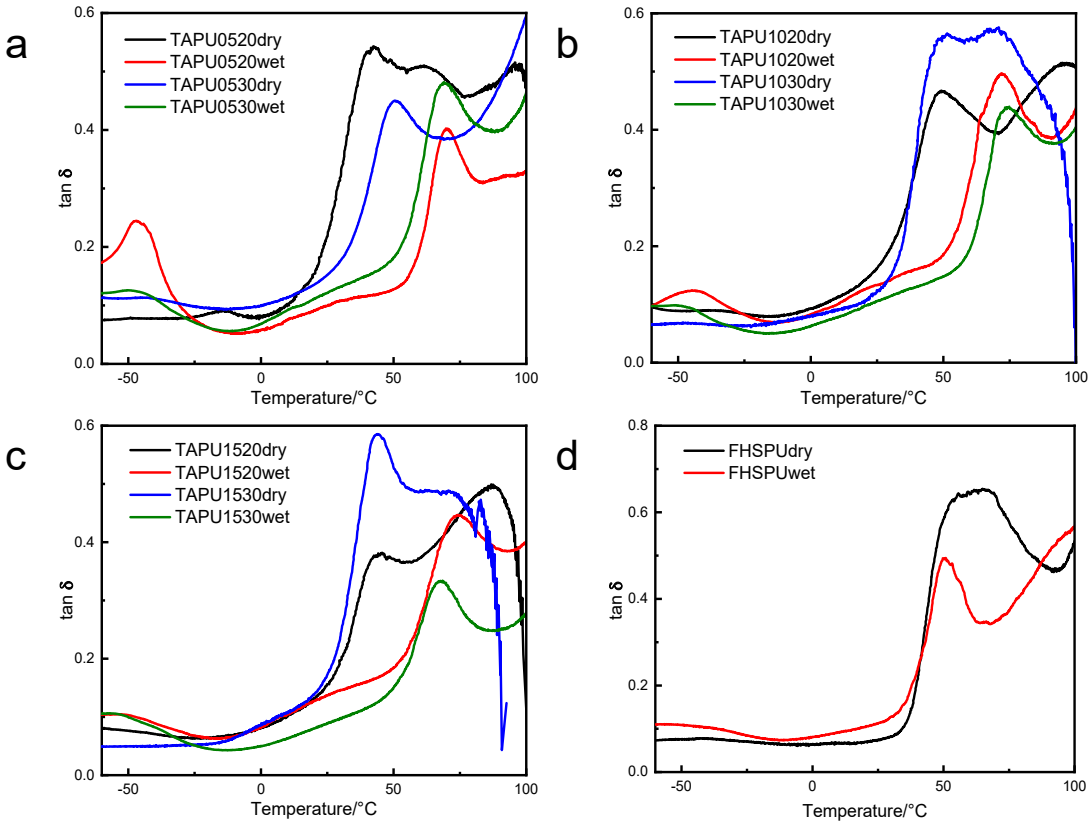

Fig. S6 Tan δ-temperature curves of FHSPU and TAPUs before and after absorbing water for 1d.

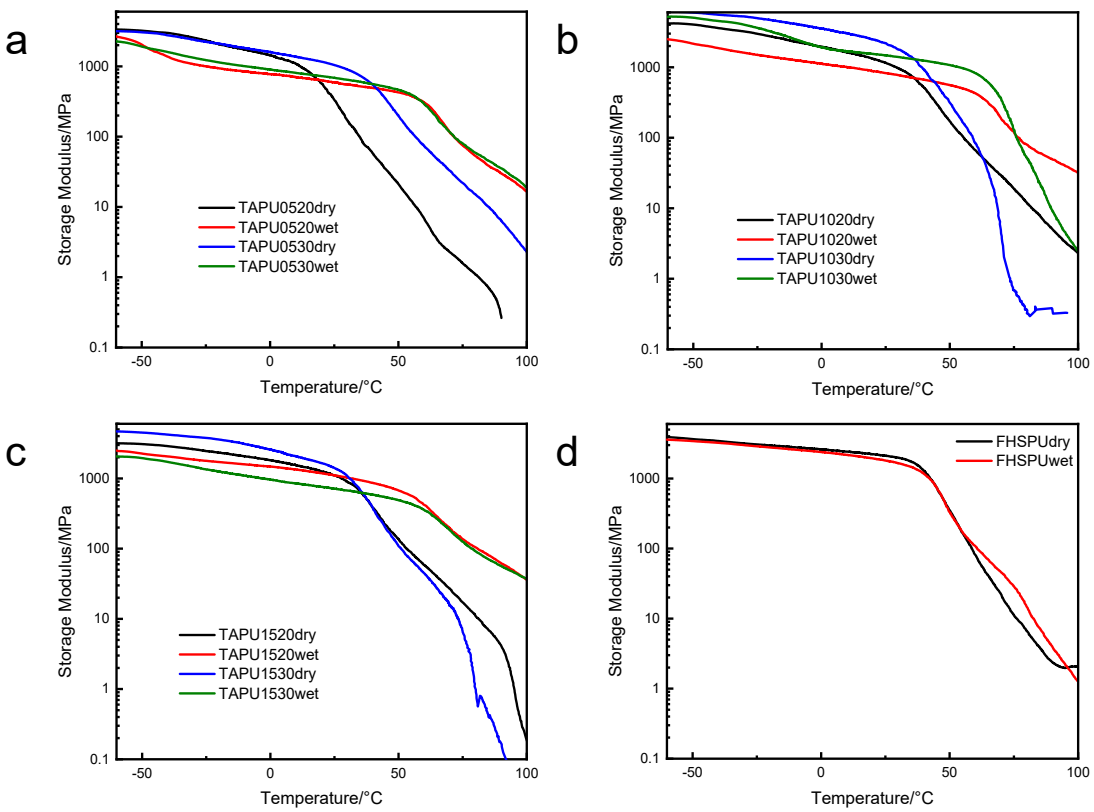

Fig. S7 Storage modulus-temperature curves of TAPUs and FHSPU of dry and wet samples.

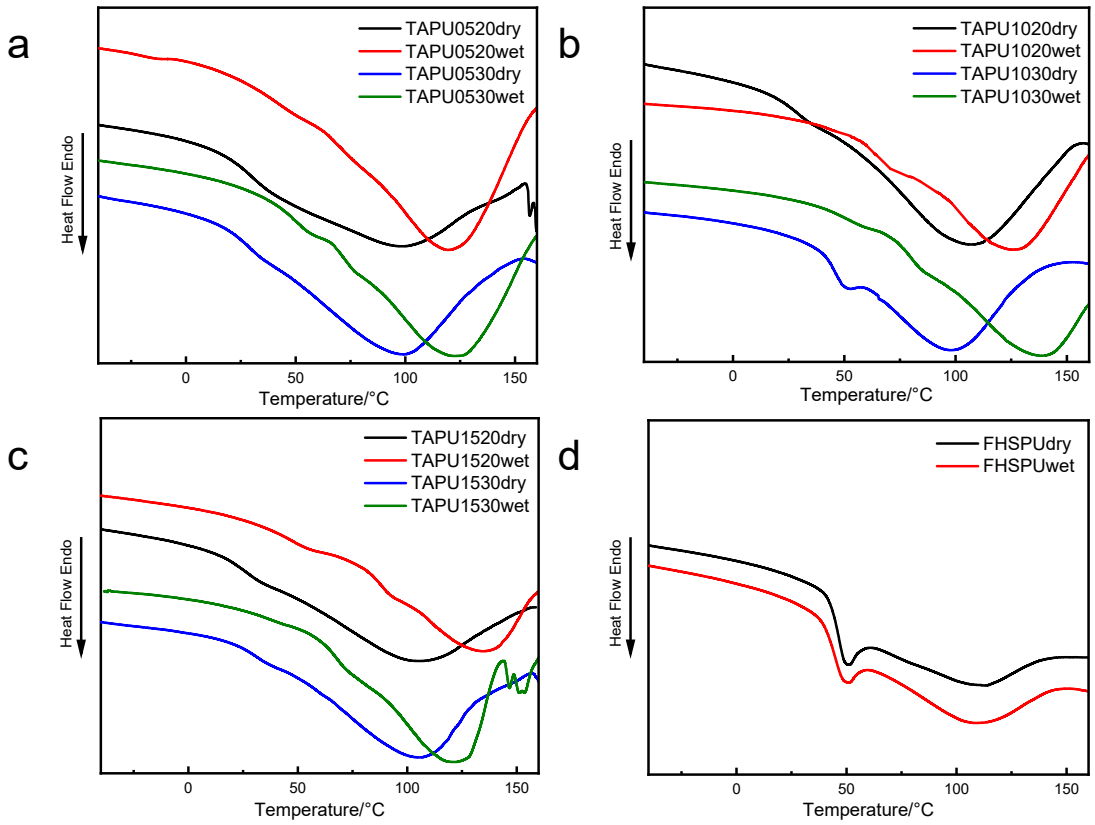

Fig. S8 DSC curves of FHSPU and TAPUs of dry and wet samples (wet samples were tested after absorbing water for 1 d and being freeze-dried).

Table S2 T_g and T_m of TAPUs and FHSPU.

Sample	T_g by DMA/°C			T_m by DSC/°C		
	Dry state	Wet state	ΔT_g*	Dry state	Wet state	ΔT_m#
TAPU0520	42.91	69.69	26.78	98.77	111.03	12.26
TAPU0530	50.61	68.83	18.22	99.91	125.87	25.96
TAPU1020	49.19	71.87	22.68	105.93	139.85	33.92
TAPU1030	51.41	74.82	23.41	98.81	142.37	43.56
TAPU1520	45.70	74.09	28.39	105.22	135.85	30.63
TAPU1530	43.92	68.46	24.54	104.26	122.89	18.63
FHSPU	64.81	50.84	-13.97	112.19	109.87	-2.32

*:ΔT_g = T_g (Wet state) - T_g (Dry state)

#:ΔT_m = T_m (Wet state) - T_m (Dry state)

The value of T_g in the table is obtained from the tan δ-temperature curves obtained by DMA rather than the results of DSC because the wet samples cannot be well obtained due to the influence of water that they only can be tested after being freeze-dried for DSC test, while the plasticization of water will not exist after freeze-drying so the T_g of freeze-dried samples cannot reflect the T_g of wet samples. The value of T_m in the table is obtained from the results of DSC, because the dry samples become soft and will slip above 100°C that the value of T_m can't be well obtained from the tan δ-temperature curves obtained by DMA, while the temperature in the freeze-drier is obviously lower than the T_m of PUs that freeze-drying has little effect on the crystalline region so the T_m of freeze-dried samples can reflect the T_m of wet samples to a certain extent[14].

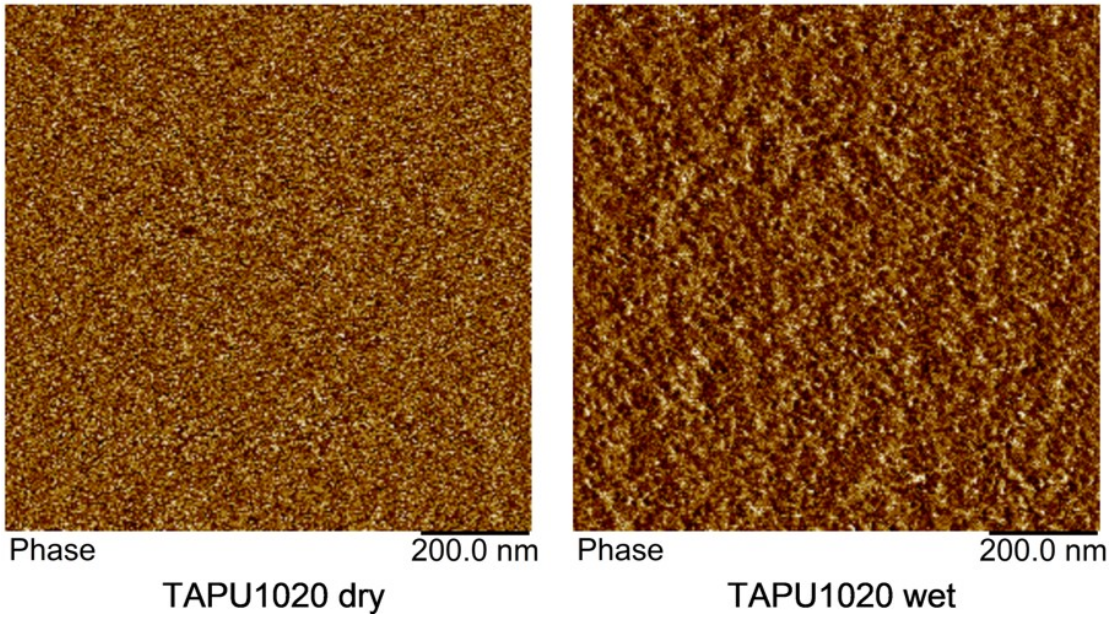

Fig. S9 Phase image of TAPU1020 acquired by AFM (tapping mode) before and after absorbing water.

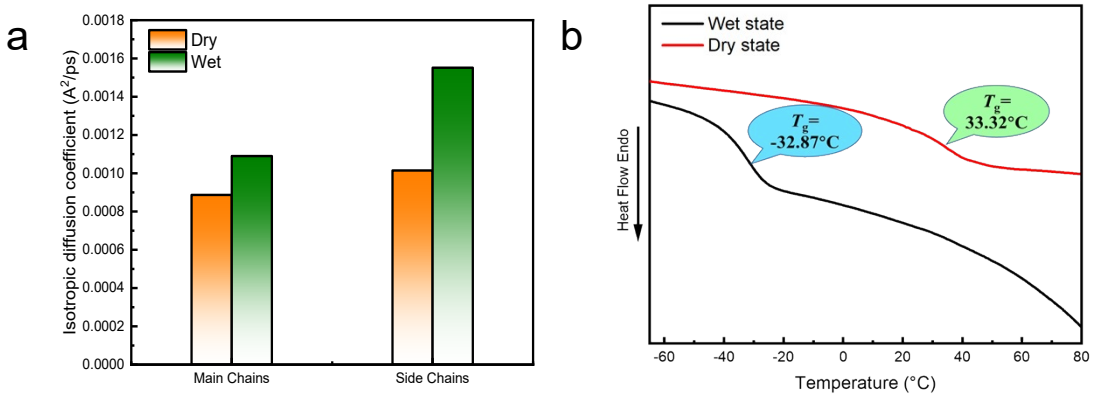

Fig. S10 (a) Isotropic diffusion coefficient of TAPU1020 in air and water. (b) T_g of PDMAPAA1000 before and after humidity treatment. (Dry PDMAPAA1000 was put in an 80% constant humidity environment for 1 d before DSC test, the temperature was raised from -80 °C to 150 °C at 10 °C/min and maintained for 20min for water removal, reduced the temperature to -80 °C and then raised the temperature to 150 °C at 10 °C/min, take T_g obtained from the first heating as T_g of hydrated PDMAPAA1000, and T_g obtained from the second heating as T_g of dry PDMAPAA1000.)

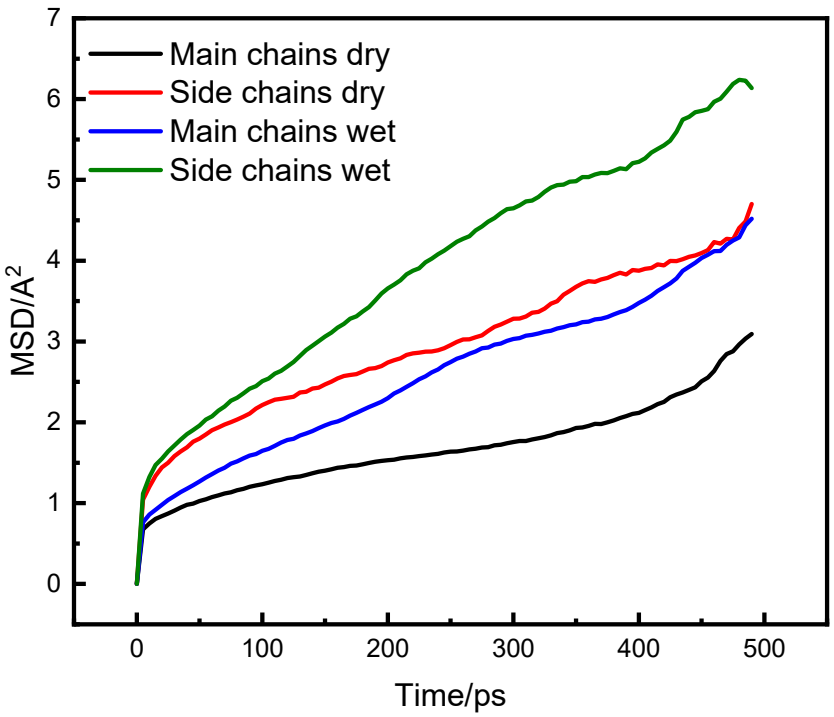

Fig. S11 MSDs of main chains and side chains as a time function.

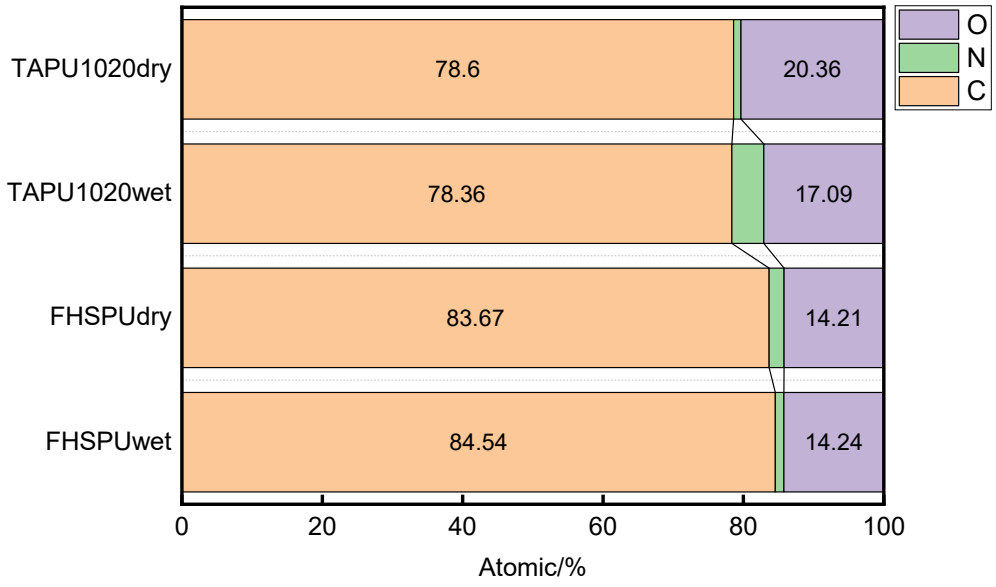

Fig.S12 Element contents of FHSPU and TAPU1020 before and after absorbing water.

The content of N in the side chains PDMAPAA (about 18.2% in theory) is higher than that of the main chains (about 7.63% in theory) and the content of O in the side chains PDMAPAA (about 9.1% in theory) is less than that of the main chains (about 18.32% in theory) for TAPU. The increase of N and the decrease of O for TAPU1020 after immersing in water and being freeze-dried is attributed to the migration of hydrophilic side chains to the surface driven by the spontaneous segment rearrangement under the hydrophobic-hydrophilic interaction of water.

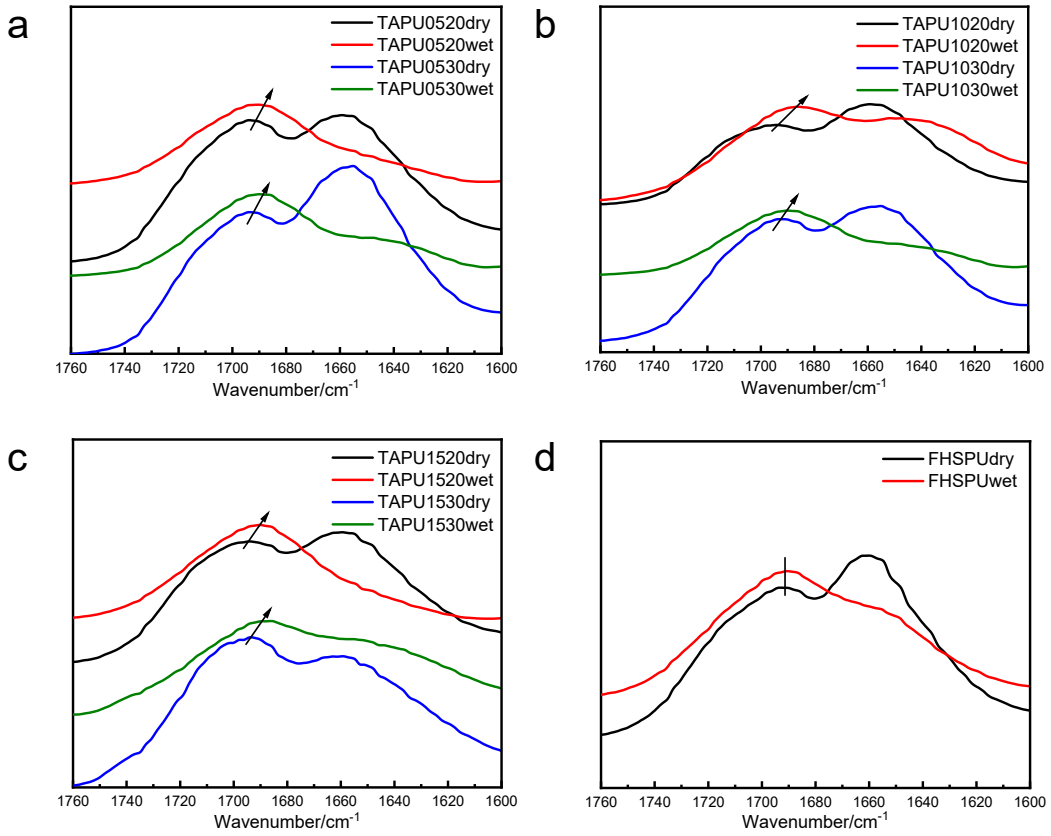

Fig. S13 ATR-FTIR curves of FHSPU and TAPUs.

Table S3 Water absorption of all samples

Samples	Water absorption/%	
	Room temperature (23°C)	Physiological temperature (37°C)
TAPU0520	18.23±0.74	21.25±0.98
TAPU0530	20.86±0.79	24.02±1.02
TAPU1020	19.17±0.66	20.98±0.88
TAPU1030	24.29±1.03	26.24±0.91
TAPU1520	23.21±0.94	26.39±1.14
TAPU1530	31.9±0.82	32.34±1.26
FHSPU	6.25±0.32	7.96±0.43

The modulus of TAPU1530 didn't increase after absorbing water at room temperature for its high water absorption and stronger plasticizing effect of water. For all the TAPUs, it was almost in the range of glass transition at 37°C for dry samples, so the mechanical properties at 37°C decreased significantly for dry samples. While T_g of them increased significantly after absorbing water, and they even hadn't reached their glass transition range at 37°C, so the mechanical properties for wet samples at 37°C were greatly improved compared with dry samples that even TAPU1530 showed better mechanical properties after absorbing water at physiological temperature.

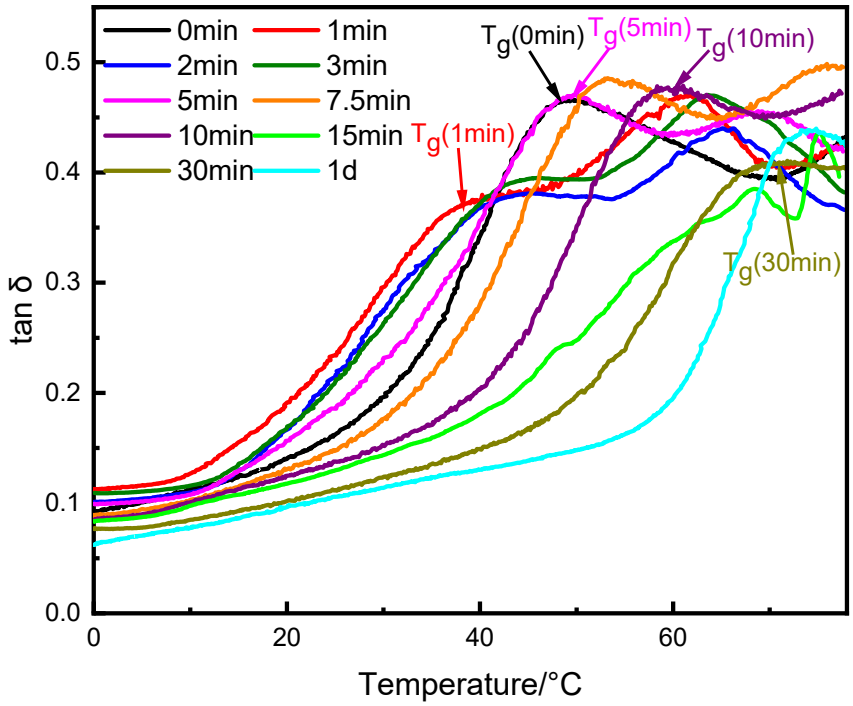

Fig. S14 Tan δ-temperature curves of TAPU1020 during absorbing water versus the immersion time at 23 °C.

Table S4 Young's Modulus and R_r of the control PEGPU.

Contents of PEG side chains / %	Young's Modulus / MPa				R_r / %			
	23D	23W	37D	37W	23D	23W	37D	37W
12.3	600±34	403±22	359±22	267±16	22.6±1.9	39.8±2.7	44.1±3.2	60.9±4.3

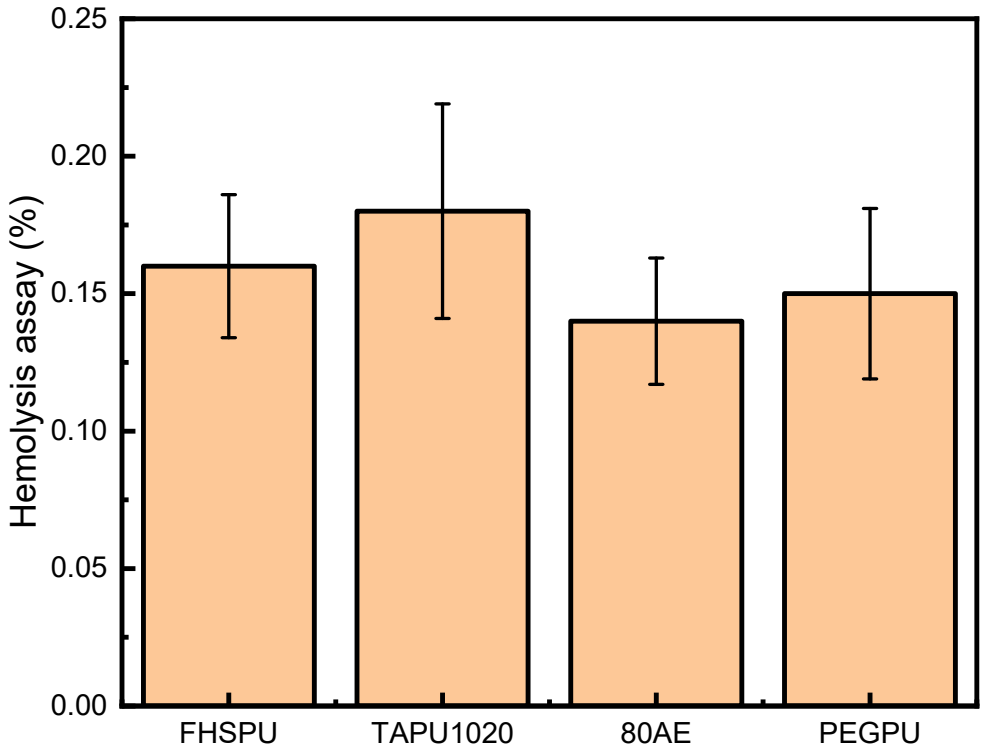

Fig. S15 Hemolysis rate of PUs.

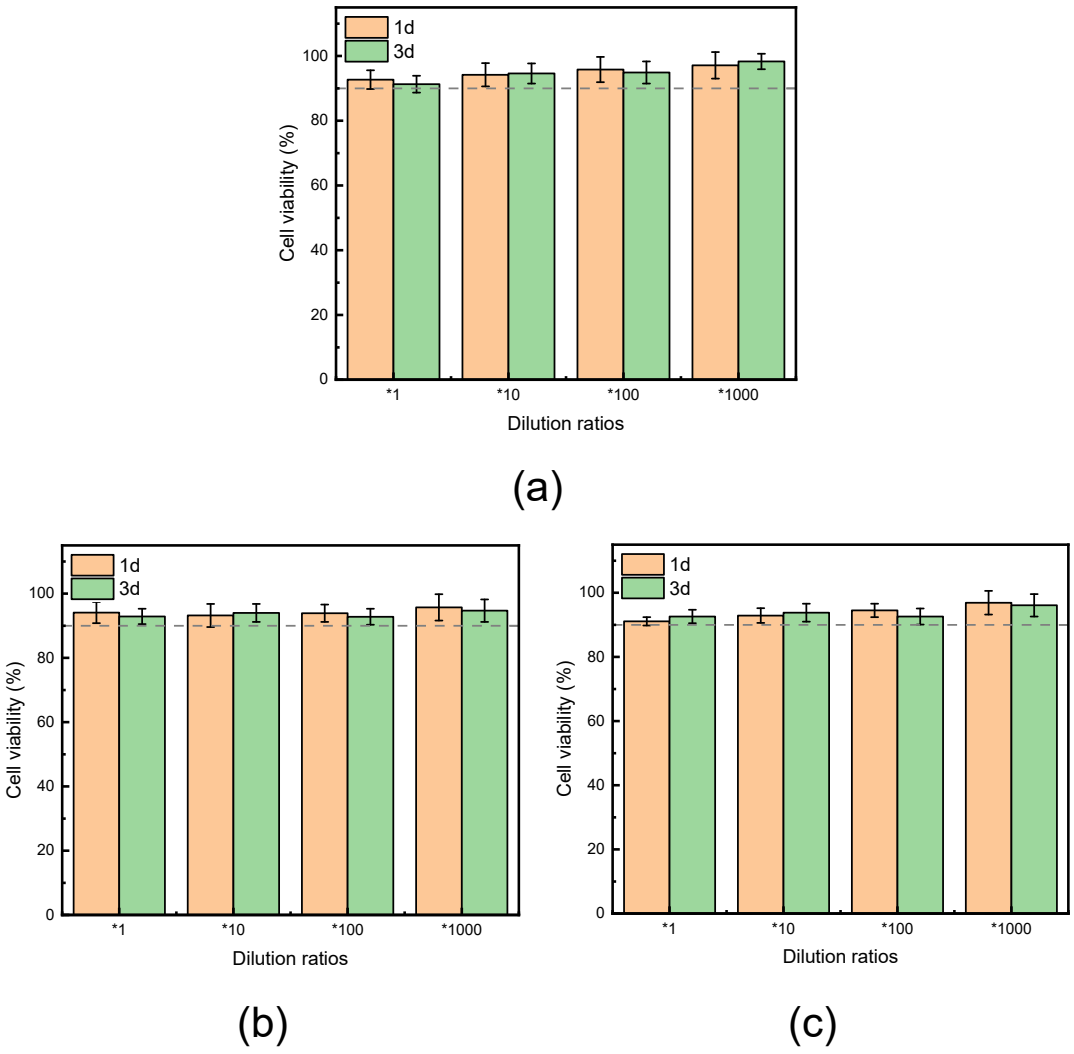

Fig. S16 Cell viability (L929) after 1d and 3d exposure to various concentrations of (a) TAPU1020; (b) FHSPU and (c) PEGPU film extracts.

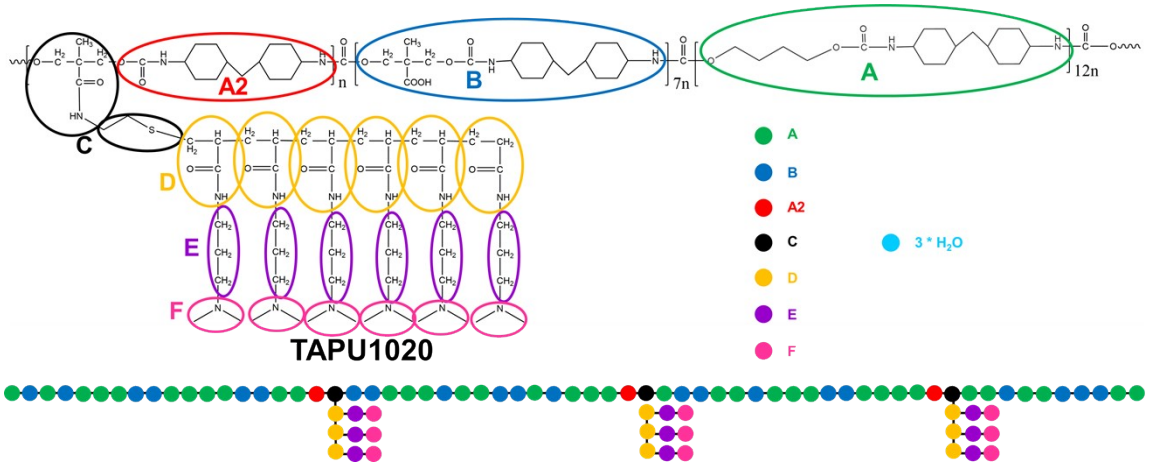

Fig. S17 Chemical structures and corresponding coarse-grained models of simulated systems.

Table S5 Solubility parameter of the beads.

beads	Solubility parameter
A	19.83
A2	18.811
B	21.293
C	22.105
D	28.028
E	16.629
F	25.684
W	46.807

Table S6. Calculated α_{ij} (upper diagonal) of the beads.

	A	A2	B	C	D	E	F	W
A								
A2	32.85							
B	41.92	28.05						
C	42.75	28.69	25.24					
D	59.04	48.94	39.10	30.42				
E	33.54	26.25	31.34	29.06	35.04			
F	29.71	37.44	30.63	26.74	25.42	29.82		
W	267.05	235.99	219.17	111.67	54.56	83.87	54.14	

References

1. R. D. Groot and P. B. Warren, *J. Chem. Phys.*, 1997, **107**, 4423-4435.
2. R. D. Groot and T. J. Madden, *J. Chem. Phys.*, 1998, **108**, 8713-8724.
3. S. W. Bunte and H. Sun, *J. Phys. Chem. B*, 2000, **104**, 2477-2489.
4. Y. Xu, J. Feng, H. L. Liu and Y. Hu, *Mol. Simul.*, 2008, **34**, 559-565.
5. A. Markina and A. Chertovich, *Chem. Phys. Lett.*, 2015, **624**, 74-77.
6. X. Chen, J. Zhu, Y. Luo, J. Chen, X. Ma, D. Bukhvalov, H. Liu, M. Zhang and Z. Luo, *Phys. Chem. Chem. Phys.*, 2020, **22**, 17620-17631.
7. M. J. McQuaid, H. Sun and D. Rigby, *J. Comput. Chem.*, 2004, **25**, 61-71.
8. A. Mazzone, *Int. J. Mod. Phys. C*, 2001, **12**, 31-38.
9. M. Montes-Saralegui and G. Kahl, *J. Phys.: Condens. Matter*, 2015, **27**, 325102.
10. J. E. Basconi and M. R. Shirts, *J. Chem. Theory Comput.*, 2013, **9**, 2887-2899.
11. B. Qiao, X. Zhao, D. Yue, L. Zhang and S. Wu, *J. Mater. Chem.*, 2012, **22**, 12339-12348.
12. K. Luo, W. Zheng, X. Zhao, X. Wang and S. Wu, *Materials & Design*, 2018, **154**, 312-325.
13. S. Charati and S. Stern, *Macromolecules*, 1998, **31**, 5529-5535.
14. B. Zhang, J. E. Debartolo and J. Song, *ACS Appl. Mater. Interfaces*, 2017, **9**, 4450-4456.